Support Information

Discovery of Rb-based Auric-Aurous halide perovskites as promising narrow bandgap semiconductors for energy conversion applications

Xuteng Yu[a,c,g], Chang Liu[a,b,c,d], Xifeng Fu[b], Zi-Ang Nan[f], Yuheng Li[a,b,c,d], Zilong Zhang[a,c], Qiu Xiong[c], Yingyao Zhang[c], Lingyi Meng[a,b,d,f], Shuiyang Lien[e], Peng Gao[a,b,c,d] *

a CAS Key Laboratory of Design and Assembly of Functional Nanostructures, Fujian Institute of Research on the Structure of Matter, Chinese Academy of Sciences, Fuzhou, Fujian 350002, China

b Fujian Normal University, Fuzhou 350007, China

c Laboratory for Advanced Functional Materials, Xiamen Key Laboratory of Rare Earth Photoelectric Functional Materials, Xiamen Institute of Rare Earth Materials, Haixi Institute, Fujian Institute of Research on the Structure of Matter, Chinese Academy of Sciences, Fuzhou, Fujian 350002, P.R. China

d Fujian College, University of Chinese Academy of Sciences, Fuzhou, 350002, China

e Xiamen University of Technology, Xiamen 361024, China

f Fujian Institute of Research on the Structure of Matter, Chinese Academy of Sciences, Fuzhou, Fujian 350002, P.R. China

g University of Chinese Academy of Sciences, Beijing 100049, China

Experimental characterization method

X-ray diffraction (XRD).

XRD patterns of the films were obtained from an X-ray diffractometer (Rigaku Miniflex 600, Japan) with Cu Kα radiation.

Analysis of Single Crystal Structures.

The SCs' structures were determined using a Bruker SMART APEX-II diffractometer equipped with a CCD detector (graphite-monochromatized Mo-Kα radiation, λ = 0.70 Å) at 200K. Data integration and cell refinement were performed using the APEX3 software. The structure was analyzed by direct methods and refined using the SHELXTL 97 software package. All nonhydrogen atoms of the structure were refined with anisotropic thermal parameters, and the refinements converged for $Fo^2 > 2\sigma IJFo^2$. All the calculations were performed using the SHELXTL crystallographic software package. Symmetry analysis on the model using PLATON revealed that no noticeable space group change was needed. In the refinement, the commands EDAP and EXYZ were used to restrain some of the related bond lengths and bond angles.

UV−vis−NIR Absorption and Reflection Spectra Measurements.

The UV−vis−NIR absorption and reflection spectra of powders were measured using a spectrophotometer (Agilent Cary 5000) over the spectral range of 200−1400 nm.

X-ray Photoelectron Spectroscopy (XPS) Measurements.

XPS spectra were recorded on a Thermo Scientific K-Alpha instrument operating on Al Kα = 1486.6 eV radiation with a spot size of ~200μm. Upon grinding the acquired perovskite single crystal into a fine powder, it was subsequently compressed into pellets utilizing a tablet press, yielding circular samples measuring 10 mm in diameter and 1 mm in height, designated for XPS analysis.

Thermogravimetric Analysis (TGA) Measurements.

Thermogravimetric analysis (TGA) was conducted employing a Mettler-Toledo TGA/DSC1/1600HT apparatus. The specimens were positioned within platinum crucibles and subjected to incremental heating from ambient temperature to 600°C at a rate of 5°C min^{-1} under a continuous nitrogen flow.

Computational Methods.

The first-principles density functional theory (DFT) simulations were performed with the Vienna ab initio simulation package (VASP) to study the geometric and electronic structures of the Au-based perovskites series. We adopted the Perdew–Burke–Ernzerhof (PBE)functional in the generalized gradient approximation (GGA) to optimize their geometrical structures. [1]

The spin-orbit coupling (SOC) effect is taken into account in the electronic structure calculations. The electronic constituents are 5d 6s 6p for Au, 5s 5p 6s for I, 5s 5p for

Cl, and 3p 3d for Rb. For geometric optimization, the Monkhorst–Pack k-point grid was configured as 2*9*3, while for self-consistent calculations, it was adjusted to 4*6*7. We adopted the PBE + SOC (spin–orbit coupling) function to calculate the band structures in our investigations. The projector augmented wave pseudopotentials with a cut-off energy of 520 eV were employed.

Dielectric Constant.

We utilized the Density Functional Perturbation Theory (DFPT) method to compute the dielectric function of the material. The dielectric constant, typically represented by ε, serves as a key parameter reflecting the dielectric or polar properties of piezoelectric smart materials under the influence of an electrostatic field.

$$\varepsilon(\omega) = \varepsilon_{elec}(\omega) + \varepsilon_{ion}(\omega) \#(1)$$

Carrier effective mass.

The effective mass of carriers (EMC) stands as a frequently employed metric elucidating the features of band structures. It has been widely applied across diverse domains, including versatile semiconductors and insulators. By employing the semi-classical Boltzmann transport equation for treating band structures, one can derive the effective mass of carriers. Consequently, the calculation formulas for the effective masses of electron and hole carriers (m*) are delineated below:

$$m^* = \hbar^2 \left[\frac{\partial^2 E(k)}{\partial^2 k} \right]^{-1} \#(2)$$

In this context, *E(k)* denotes the energy dispersion function delineated by the band, and $\hbar$ signifies the Planck constant. The magnitude of the effective mass is dictated by the local curvature of the band extrema: lesser curvature corresponds to a greater effective mass, whereas greater curvature corresponds to a lesser effective mass.[2]

Exciton Binding Energy.

The binding energy (E_b) of excitons refers to the minimum energy required for the separation of electron-hole pairs, allowing them to move to their respective electrodes and generate current in solar cells. Smaller binding energy implies a more significant energy difference between electrons and holes, making it less likely for them to recombine and produce additional free electrons. To study the feasibility of exciton separation in the absorber material of a solar cell, the hydrogen-like Wannier-Mott exciton model is commonly used to calculate the exciton binding energy. The equation for the exciton binding energy is given by:

$$E_b = \frac{\mu^* R_y}{m_0 \varepsilon_r^2}$$

$$\frac{1}{\mu^*} = \frac{1}{m_e} + \frac{1}{m_h} \#(3)$$

where R_y is the Rydberg energy of an atom, ε_r is the relative dielectric constant (i.e., the high-frequency limit of the dielectric constant after electron polarization). The value of exciton binding energy is the difference between the optical bandgap and the electron bandgap.[3]

Optical Absorption Coefficient.

The optical absorption coefficient (α) is the total absorption area per unit volume of a medium and can describe the intensity attenuation when light enters the material. The calculation formula is as follows:

$$\alpha = 2\omega\left[\frac{\left(\varepsilon_1^2(\omega) + \varepsilon_2^2(\omega)\right)^{\frac{1}{2}} - \varepsilon_1(\omega)}{2}\right]^{\frac{1}{2}} \#(4)$$

Here, $\varepsilon_1(\omega)/\varepsilon_2(\omega)$ are the real/imaginary parts of the dielectric function. The imaginary part of the dielectric function is calculated using the random phase approximation, while the real part is obtained from the imaginary part according to the Kramers-Kronig relations.[4]

Thermoelectric Property.

All the calculations based on the density functional theory (DFT) and the Projector Augmented Wave (PAW) potential were implemented with the Device Studio,[5], which provides a number of functions for performing visualization, modeling, and simulation. Structural optimization using DS-PAW code[6] code integrated into the Device Studio program. The generalized gradient approximation in the Perdew-Burke-Ernzerhof (PBE) format was used to compute exchange and correlation energies, and a plane wave basis set cut-off energy of 600 eV was adopted. Grimme's DFT-D3 was used for dispersion correction. To avoid imaginary frequency, A mesh of 16×16×14 Gamma-centered k-points was used for the Brillouin-zone integration. The criterion of electron self-consist iteration was set as 1.0×10^{-9} eV, and the maximum force was relaxed down to 1.0×10^{-4} eV $Å^{-1}$.

Thermoelectric properties were simulated using Nanodcal code7, which is based on non-equilibrium Green's function density functional theory (NEGF-DFT). We used 2*2*2 supercells to calculate the Phonon part. LDA-PZ81 was employed as the exchange-correlation functional, and the cut-off energy was set to 80 Hartee. The criterion of electron self-consist iteration was set as 1.0×10^{-12} eV.

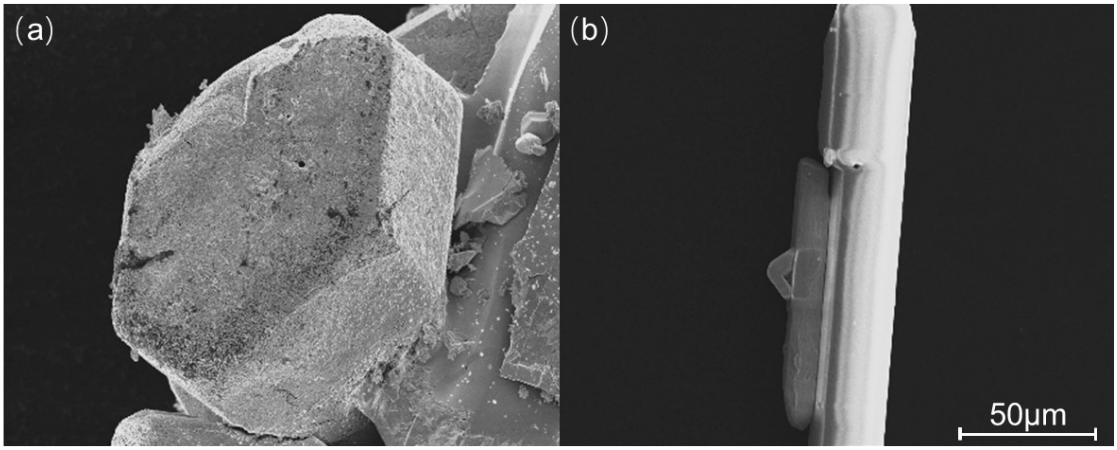

Fig S1. SEM image (2500×) of $Rb_2Au_2I_6$ (a) and $RbAuCl_4$(b).

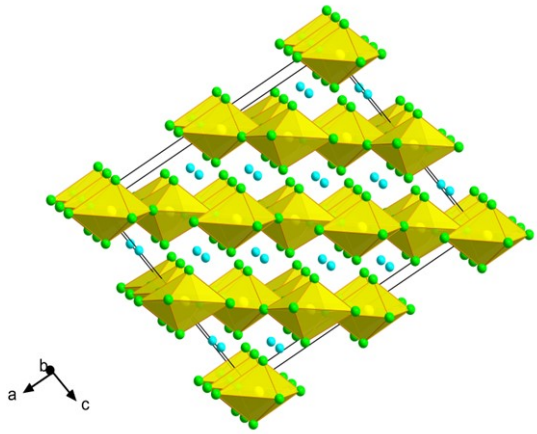

Fig S2. The schematic diagram of the 2×2×2 single crystal structure of $RbAuCl_4$ with (010) direction. The diagram clearly illustrates the ordered disposition of Rb^+ ions, effectively partitioning the $[AuCl_6]^{3-}$ octahedral layers and thereby engendering the emergence of a 2D RP perovskite structure.

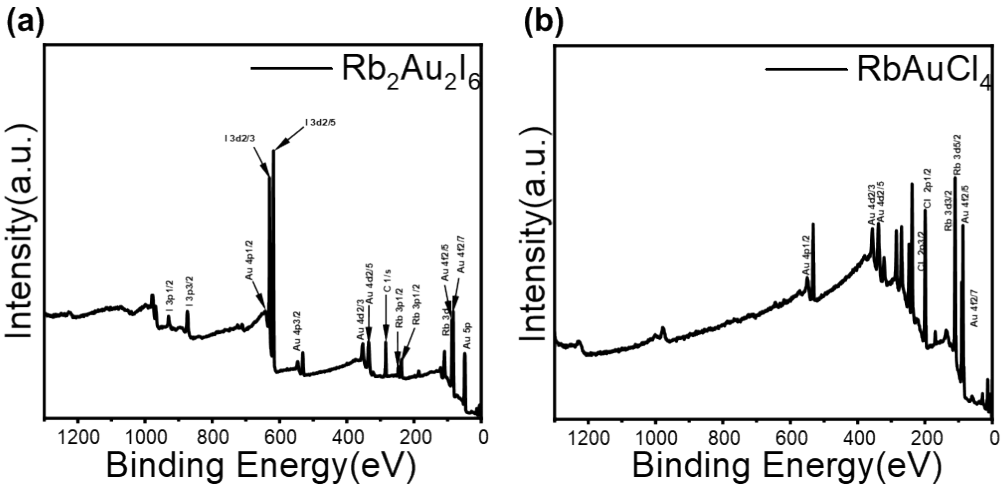

Fig S3. Survey scan of XPS spectra for the (a) $Rb_2Au_2I_6$ and (b) $RbAuCl_4$.

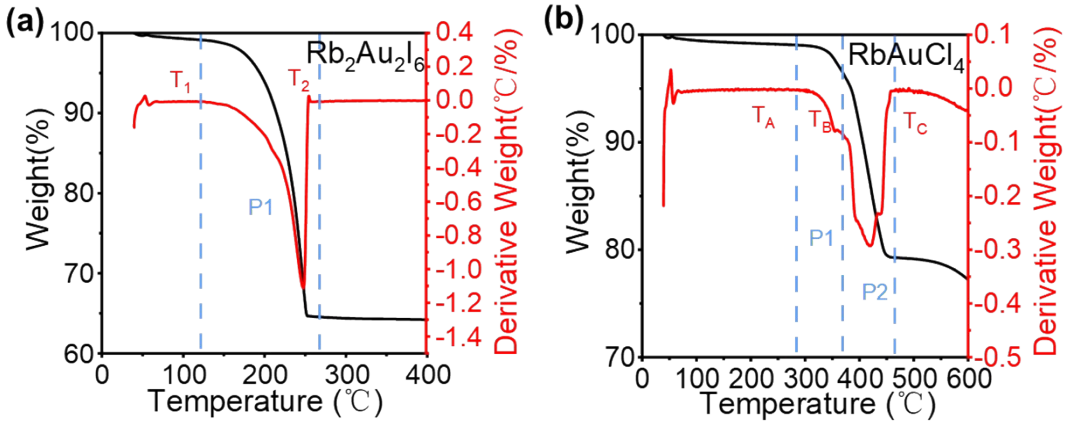

Fig S4. TGA (black) and DTG (red) curves for (a) $Rb_2Au_2I_6$ and (b) $RbAuCl_4$.

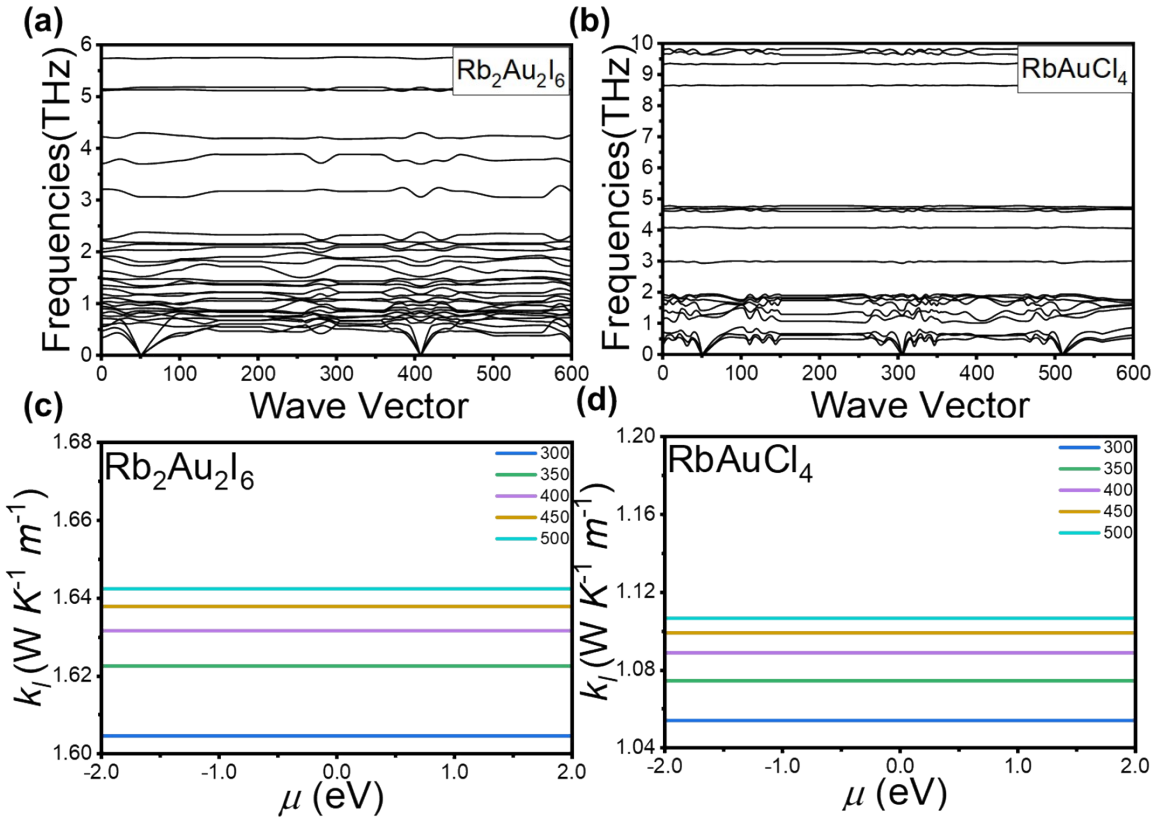

Fig S5. Phonon spectra of $Rb_2Au_2I_6$ (a) and $RbAuCl_4$(b); Lattice electrical conductivity(κ_l) of $Rb_2Au_2I_6$ (c) and $RbAuCl_4$ (d).

Table S1. Crystal data and structure refinement of $RbAuCl_4$, $Rb_2Au_2I_6$

	$RbAuCl_4$	Rb_2Au2I_6
Empirical formula	$RbAuCl_4$	$Rb_{0.5}Au_{0.5}I_{1.5}$
Formula weight	424.24	331.57
Temperature [K]	200.00	200.00
Crystal system	monoclinic	monoclinic
Space group(number)	C2/c (15)	C2/m (12)
a [Å]	20.8939(8)	13.4470(15)
b [Å]	5.8513(2)	7.8726(9)
c [Å]	17.3064(6)	8.7665(9)
α [°]	90	90
β [°]	100.050(2)	119.300(6)
γ [°]	90	90
Volume [Å3]	2083.35(13)	809.32(16)
Z	12	8
ρcalc [$g \cdot cm^{-3}$]	4.058	5.442
μ [mm^{-1}]	29.555	35.482
F (000)	2208	1100
Crystal color	yellow	Black
Crystal shape	block	Polyhedron
Radiation	MoKα (λ=0.71073 Å)	MoKα (λ=0.71073 Å)
2θ range [°]	3.96 to 54.99 (0.77 Å)	5.33 to 57.54 (0.74 Å)
Index ranges	$-26 \le h \le 26$	$-18 \le h \le 18$
	$-7 \le k \le 7$	$-10 \le k \le 10$
	$-22 \le l \le 22$	$-11 \le l \le 11$
Data / Restraints / Parameters	2395/0/84	1130/0/30
Absorption correction	0.4272/0.7462	0.4751/0.7458
Tmin/Tmax (method)	(none)	(none)
Goodness-of-fit on F2	0.920	1.148
Final R indexes	R1 = 0.0428	R1 = 0.0341
[I≥2σ(I)]	wR2 = 0.1363	wR2 = 0.0775
Final R indexes	R1 = 0.0749	R1 = 0.0550
[all data]	wR2 = 0.1551	wR2 = 0.0929
CCDC No	2363017	2341967

Table S2. The calculated band gaps (E_g), electron, and hole effective masses (m_e, m_h) reduced exciton mass(μ*), dielectric constants(ε), and exciton binding energies (Eb) of $Rb_2Au_2I_6$ and $RbAuCl_4$.

Compound	E.g. (eV)	$m_e^*(m_0)$	$m_h^*(m_0)$	μ*	ε	Eb(eV)
	PBE+SOC					
$Rb_2Au_2I_6$	0.69	0.314	0.847	0.23	6.83	0.067
$RbAuCl_4$	1.95	5.56	0.51	0.47	3.21	0.62

REFERENCES

(1) Perdew, J. P.; Burke, K.; Ernzerhof, M. Generalized *Phys. Rev. Lett.* **1996**, *77* (18), 3865–3868.
(2) Wyman, M.; Pogosian, L.; Wasserman, I. **2005**, *72* (2), 023513.
(3) Zhu, X.; Su, H.; Marcus, R. A.; Michel-Beyerle, M. E. *J. Phys. Chem. Lett.* **2014**, *5* (17), 3061–3065.
(4) Gajdoš, M.; Hummer, K.; Kresse, G.; Furthmüller, J.; Bechstedt, F. *Phys. Rev. B* **2006**, *73* (4), 045112.
(5) Hongzhiwei Technology. Available online:https://iresearch.net.cn/cloudSoftware.
(6) Blöchl, P. E. *Phys. Rev. B,* **1994**, *50* (24), 17953–17979.